Thin Solid Films 838 (2026) 140898

Contents lists available at ScienceDirect

Thin Solid Films

journal homepage: www.elsevier.com/locate/tsf

Investigating composition-dependent fracture toughness in silicon-rich silicon nitride layers

Filippo Sabatini [a,*], Emanuele Cattarinuzzi [b], Vincent Coutellier [c], Andrea Serafini [b], Simone Mariani [b], Davide Fagiani [b], Laurent-Luc Chapelon [c], Paola Zuliani [b], Andrea Li Bassi [a]

[a] Department of Energy, Politecnico di Milano, via Lambruschini, 20156 Milano, Italy
[b] STMicroelectronics Agrate, Camillo Olivetti 2 - 20864 Agrate Brianza, MB, Italy
[c] STMicroelectronics Crolles, imm Belledonne 1 - 850 r Jean Monnet, 38920 Crolles, France

ARTICLE INFO

Keywords:
Passivation
Toughness
Surface characterization
Nanoindentation

ABSTRACT

This study systematically investigates the mechanical properties, particularly fracture toughness, of plasma enhanced chemical vapor deposited SiN_x films by exploring variations in their chemical composition. Three films with sub-micrometer thickness (600 nm) and different stoichiometry, i.e., increasing silicon content, were deposited and characterized by X-ray photoelectron spectroscopy, Raman and photoluminescence spectroscopy, and transmission electron microscopy. Mechanical properties were determined using nanoindentation, applying the Oliver–Pharr method for hardness and elastic modulus and a procedure suitable for thin films, developed by Xia et.al., for fracture toughness measurement. Results revealed an enhancement in fracture toughness for the highest silicon-content film, while the intermediate sample showed no significant variations, suggesting the existence of a silicon-content threshold above which some toughening effect is initiated. The observed toughening mechanism is hypothesized to be related to the substantial dispersion of amorphous silicon heterogeneities, affecting intrinsic stress evolution and mechanical compliance of the films. These findings highlight the critical role of chemical composition and microstructural features in controlling mechanical performance and provide valuable guidelines for the customization of SiN_x passivation layers in the semiconductor industry.

1. Introduction

Silicon nitride (SiN_x) thin films deposited via Plasma Enhanced Chemical Vapor Deposition (PECVD) are widely employed as passivation and dielectric layers in advanced semiconductor devices, owing to their excellent combination of chemical inertness, electrical insulation, mechanical robustness, and thermal stability [1–4]. Despite these advantageous properties, one critical limitation of SiN_x layers is their brittle post-elastic behavior [5,6], which represents a primary concern within the semiconductor industry, as it implies cracking as the primary mechanism for dissipation of excess strain energy developed due to thermomechanical stresses typical of electronic devices production steps [5].

For this reason, the assessment of fracture toughness is a key step for the mechanical characterization of ceramic passivation layers, such as SiN_x. This property quantifies the material resistance to crack propagation and is therefore a decisive parameter for evaluating the reliability and lifetime of the semiconductor device [7,8]. However, the accurate measurement of fracture toughness in thin films, especially those with thickness below 1 μm, presents significant experimental challenges. Conventional methods such as the Lawn–Evans–Marshall (LEM) approach, which rely on indentation-induced crack patterns, become problematic due to substrate effects and crack propagation into the underlying silicon substrate, making the derived values unreliable for sub-micrometer films [9,10].

In recent years, several methods have emerged as alternative techniques specifically designed to overcome these limitations for thin and brittle coatings. Micro-pillar splitting, micro-cantilever bending, and micro-chevron beam, have been developed to accurately measure fracture toughness in thin films; however, these methods must be often supported by complex sample preparation or finite element simulations [7,8,11,12]. In contrast, Xia et.al. have developed a method which involves simpler sample patterning, offering a practical alternative for assessing thin-film toughness based on an energy balance approach [13,14]. With this method the interference of the substrate effects is excluded, by requiring a simple patterning of the film deposited. More

* Corresponding author.
E-mail address: filippo.sabatini@polimi.it (F. Sabatini).

https://doi.org/10.1016/j.tsf.2026.140898
Received 13 October 2025; Received in revised form 6 February 2026; Accepted 24 February 2026
Available online 25 February 2026

details of this characterization method will be discussed in the section "Methodology".

Concerning the approaches to limiting the brittle failure, it is known that, by controlling the development of residual stresses, it is possible to modify the final toughness of the material [15]. Residual stresses develop naturally during the PECVD deposition process, because of thermal expansion mismatches, plasma-induced ion bombardment, and chemical gradients within the growing film. Depending on process conditions these stresses can manifest either tensile or compressive, respectively reducing or enhancing the effective toughness of the film by promoting or preventing crack initiation and propagation. Nevertheless, the mechanisms underlying the formation and control of residual stresses in SiN_x films are still not fully understood, particularly when dealing with thin layers [15]. Thus, investigating the effect of varying chemical composition in thin SiN_x layers can be the most effective way of influencing their mechanical properties [1,16,17]. For example, by increasing relative gas flows of silane (SiH_4) with respect to ammonia (NH_3) during PECVD the spontaneous formation of amorphous silicon nanoparticles (NPs) embedded in the SiN_x matrix is observed [16–20]. Such composition is generally referred to as "silicon rich" (SR) silicon nitride, and whether these embedded NPs could offer meaningful contributions to mechanical properties is still an information subject to research.

The present study aims to provide a comprehensive analysis of the mechanical properties of PECVD silicon nitride films, focusing on the influence of chemical composition (Si/N ratio), intrinsic stress state, and the presence and structural characteristics of embedded silicon nanoclusters. Specifically, three films with sub-micrometer thickness (600 nm) and increasing Si/N ratios were deposited via PECVD and characterized both in their chemical and mechanical properties, implementing, for the latter, the procedure developed by Xia et al. [14] to assess fracture toughness in thin films by nanoindentation.

2. Methodology

In this study, SiN_x thin films were deposited via PECVD with a nominal thickness of 600 nm on 775 um thick crystalline silicon wafers. The deposition was performed at 380 °C and 4.3 Torr for all samples, exploiting different gas mixtures varying the silane (SiH_4) flux while maintaining a fixed ammonia (NH_3) flux. Three primary compositions were selected for investigation: a quasi-stoichiometric silicon nitride film, deposited with a silane/ammonia flux ratio equal to 3:4 and labelled as "St" (Standard), and two silicon-rich variants with silane/ammonia flux ratio equal to 4:1 and 5:1, referred to as "SR4" and "SR5" respectively.

Immediately after deposition, the intrinsic residual stress was determined through the application of the Stoney equation after wafer curvature measurements performed using optical profilometry [21]. After stress measurements, all wafers underwent photolithographic patterning to obtain suitable samples for mechanical characterization through the method proposed by Xia et.al [14]. Results will be discussed in Section 3.2.

Mechanical characterization was carried out using nanoindentation techniques, employing a Hysitron TI 980 TriboIndenter (Bruker, USA). Hardness (H) and plane strain elastic modulus (E_p) were determined with a Berkovich tip using the well-established Oliver–Pharr method [22] by restricting indentation depths to a range of 8 %−15 % of the film thickness and exploiting a specific analysis software, called Intrinsic Thin Film (Brucker, *Intrinsic Thin Film* Mechanical Property Solution), which implements a methodology by Li and Vlassak [23] that permits to exclude the substrate effect for a thin mono-layer deposited on a bulk substrate.

The method proposed by Xia et.al. was utilized for accurate determination of fracture toughness (K_c), which consists in using a 4-sided pyramidal tip (specifically, a Vickers geometry) to indent the substrate surface close to a free edge of the film, as schematically represented in Fig. 1.

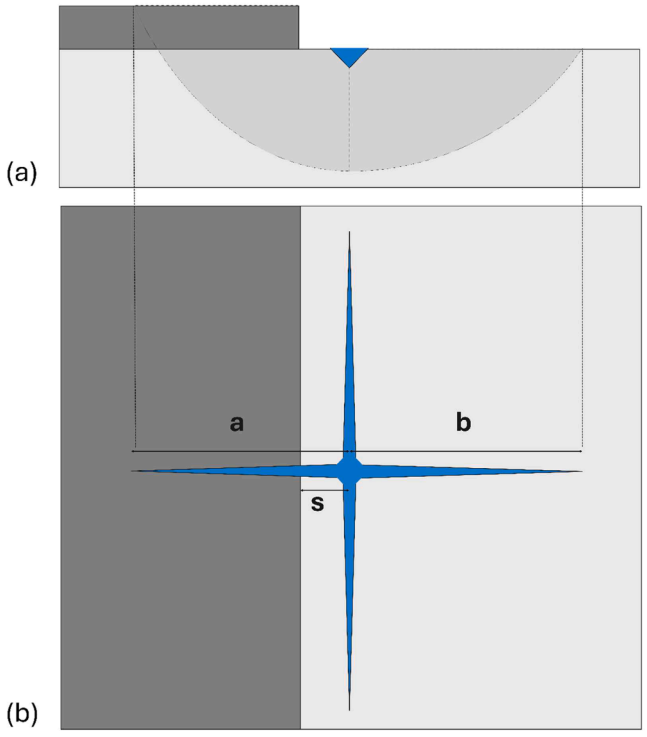

Fig. 1. schematic representation of the patterned film and indentation geometry in front view (a) and cross section (b). The Vickers tip leads to the propagation of four cracks along a cross shape. In this study we consider the two cracks normal to the film edge, designated as a for the one across the coating and b for the one across the free substrate.

This method was specifically developed to handle substrate-related effects typically encountered in thin-film fracture toughness measurements [14]. This approach involves performing an indentation with a Vickers tip on the substrate side at a distance *s* from the film. During indentation, one of the radial cracks initiates in the substrate and propagates normally toward the film and upward through its thickness, thus generating a single, clearly defined through-thickness crack with length *a*. In the opposite direction, another crack will propagate along the free substrate with length *b*. By analyzing the crack lengths produced on both coated and uncoated substrate sides, fracture toughness can be determined using an energy balance criterion, which considers the strain energy release rates for both substrate and film. The higher the toughness of the film compared to that of the substrate, the larger the difference between average *a* and *b* cracks will be, as a higher amount of the initial work generated by the indentation will be used to crack the film. The final equation to obtain the critical Stress Intensity Factor related to the toughness of the coating is expressed as:

$$K_c = \left\{ K_s^2 \left[1 + \lambda \frac{(\phi b - a)}{t} \sqrt{\frac{E_{pc}}{E_{ps}}} \right]^2 \pm \left[2\Psi_c \sigma r \sqrt{t \sqrt{\frac{E_{pc}}{E_{ps}}}} \right]^2 \right\}^{1/2} \quad (1)$$

where the subscript *c* refers to the coating film and *s* to the substrate; E_p are the respective plain strain modulus, t the coating thickness, λ and Ψ_c two dimensionless, material-independent, factors equal to 0.45 and 0.95, respectively - obtained from finite element model (FEM) calculations made by Xia et.al. in their work - and φ is the slope of the fitting obtained by plotting *a* vs *b* measured with increasing indentation loads. In this study, to obtain this last value, all samples have been indented with four different loads: 1300 mN, 1900 mN, 4500 mN and 6000 mN. An unexpected substantial challenge concerned handling the undesired failure mode from now on referred to as scaling, i.e. the partial or total

detachment of portions of the substrate near the tip imprint during the indentation process. Indeed, this competing failure mechanism is beyond the treatment of Xia et al. and has the potential to undermine the assumptions behind the energy balance of Eq. (1). For this reason, all experiments featuring scaling were discarded until we obtained 12 of them without any of these failure modes for every tested load. After indentation, the lengths of the induced cracks were characterized by optical microscopy with a Keyence VHX-7000/7000 N.

Finally, complementary structural and compositional analyses of the SiN_x films were conducted to elucidate their chemical and microstructural characteristics. X-ray photoelectron spectroscopy (XPS) was performed with a PHI5000 Versaprobe III (ULVAC-PHI) with photon energy (PE) of 280 eV, equipped with an Ar sputtering gun to perform in-depth profile analysis up to 10 μm of acquisition depth. The technique was employed to determine the accurate stoichiometry of the films, thereby verifying the intended Si/N compositional variations. Raman spectroscopy was used to probe the structural characteristics of the silicon-rich films and confirm the presence or absence of embedded silicon heterogeneities. The analysis was performed using a Renishaw InVia micro-Raman spectrometer equipped with an Ar^+ gas laser (λ=514 nm) and a 1800 grooves mm^{-1} grating. To avoid effects which could damage the samples, the incident laser power was kept <0.4 mW. With the same instrument, photoluminescence (PL) spectroscopy was performed exploiting a different laser wavelength (λ=457 nm), to assess the optical response of the Silicon-rich films, specifically looking for characteristic signals associated with quantum confinement effects from potential embedded Si NPs [17].

To provide deeper insights into the NPs potentially formed during sample deposition, the silicon-rich films were subjected to thermal annealing treatments at 1100 °C in atmosphere for 1 hour of dwell time. This thermal treatment was specifically aimed at promoting crystallization of the spontaneously formed amorphous silicon NPs within the Silicon-rich SiN_x films during their deposition. This operation was necessary to allow direct observation of the NPs by transmission electron microscopy (TEM), which was otherwise not able to distinguish the NPs in their amorphous state from the amorphous SiN_x matrix. The measurements were conducted on electron transparent lamellae, using a Thermo Fisher Themis Z aberration-corrected Scanning Transmission Electron Microscope (STEM), operating at 300 kV acceleration voltage. Dark-Field TEM (DF-TEM) images were acquired on the annealed samples for microstructural analysis and determination of crystal dimensions, providing an independent means of verifying and quantifying the NPs size and distribution, as previously inferred from Raman and PL analyses. Moreover, the images were taken in two areas, one near the substrate and the other near the surface of the SiN_x films, to observe possible gradients in the NPs distributions and average diameters along the film thickness. Finally, to avoid observing the oxidized thickness of the SiN_x films after the annealing, estimated to be lower than 100 nm [24], the set of figures near the surface was taken under this outermost thickness.

3. Results

3.1. Structural characterization of silicon nitride films

Initially, XPS measurements were employed to determine the chemical composition of the as-deposited films. Fig. 2 illustrates the atomic percentages of silicon and nitrogen on the left, and the Si/N atomic ratio on the right, for increasing flux of the silane precursor gas considering a fixed ammonia flux. Depth profiling by Argon sputtering showed constant Si/N atomic ratios for the three films, equal to 0.86, 1.10 and 1.33 for the St, SR4 and SR5, respectively. Moreover, no other elements than silicon or nitrogen were detected.

Several differences related to stoichiometry variation can be observed in the spectra resulting from Raman analysis, reported in Fig. 3. Firstly, it is possible to observe a variation in the transparency of

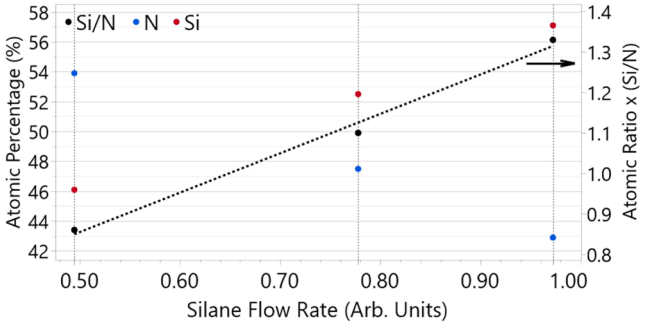

Fig. 2. XPS results reporting atomic percentages of Si and N atomic content on the left and Si/N atomic ratio on the right. Results are reported for increasing silane flow rate during PECVD deposition considering a fixed ammonia flux. The dashed line is a reference for qualitative comparison with the data, suggesting the Si/N atomic ratio grows rather linearly with the Silane flow rate.

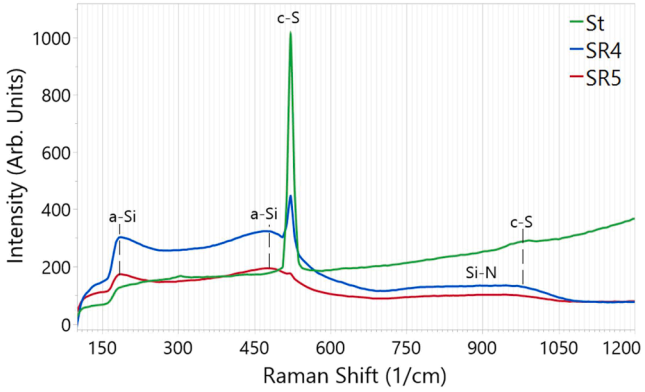

Fig. 3. Raman spectra of St, SR4 and SR5 SiNx. The two silicon rich samples show bands related to amorphous silicon content which are not present in the Standard sample. The strong peak related to crystalline silicon origin from the substrate and its decreasing intensity for the three samples indicates a lower transparency of the SiNx films for increasing silicon content during PECVD deposition.

the three characterized films, which decreases with increasing silicon content. This can be observed by the decreasing intensity of the crystalline silicon peak, positioned at 521 cm^{-1}, which originates from the substrate. Since the three films have the same thickness, the lower intensity of the peak indicates lower transparency (or higher absorbance) with increasing silicon content. Moreover, the standard film shows no other distinct signal in the observed range, except for the initial part of a photoluminescence broad band. This last effect partially covers a band, ranging from 750 to 1000 cm^{-1}, related to Si-N vibrational modes of silicon nitride [18,25] which is observable for the two silicon rich samples, whose photoluminescence effects begin for higher Raman shifts, as it will be discussed later. Opposite to the St sample, the SR4 and SR5 samples show distinct vibrational features associated with localized amorphous silicon domains. Specifically, a broad band around ~470 cm^{-1} is generated by the characteristic signal of Si-Si stretching mode at 465 cm^{-1} and the transverse optical (TO) band of amorphous silicon at 480 cm^{-1} [18,19,26]. Other known signals related to amorphous silicon are responsible for the band positioned at 180 cm^{-1}, further indicating the presence of heterogeneities dispersed in the SiN_x matrix spontaneously formed during deposition [17,25,27]. These Si heterogeneities seem to be present only in silicon rich samples since no signal related to amorphous silicon is visible for the St sample.

Complementary to Raman spectroscopy, photoluminescence measurements provided additional information related to the Si NPs presence. PL spectra of all the samples analyzed are shown in Fig. 4 reported

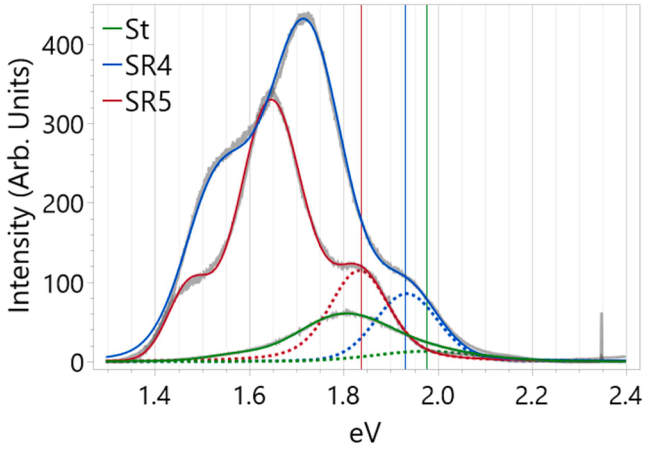

Fig. 4. Spectrum of photoluminescence obtained for the three samples reported with black and colored solid lines for the original and fitting curves, respectively. The dotted lines represent the deconvoluted peaks related to quantum confinement effect. The central energy values of such peaks are linkable to the average dimension of the amorphous silicon heterogeneities: the lower the PL energy, the bigger the heterogeneity. Moreover, higher relative intensities indicate higher presence of emitters, i.e. heterogeneities, embedded in the SiNx matrix.

with black and colored solid lines for the original and fitting curves, respectively. It is well established that silicon nitride PL signal can vary strongly with different synthesis methods and deposition parameters [28,29]: the spectra are composed of several contributions due to the different defect states in the bulk material, band-tail effects, and possibly quantum confinement effects related to the NPs presence [30–32].

The fittings shown in Fig. 4 for each original photoluminescence signal were obtained employing the software Fytic, which permits to evaluate the weighted sum of squared residual (WSSR) of the curves. For each sample, a very good WSSR value (1 ± 0.1) has been obtained for the relative fitting, achieved by performing a deconvolution of the original curve using three peaks described by a Voigt function (Gauss-Lorentzian Function). Similar results have been observed in other studies that associate the two lower-energy peaks with radiative defect states and band tail effects [17,19,31], and the higher-energy peak, in the range from 1.8 to 2.1 eV, with quantum confinement by Si clusters and, thus, with the presence of NPs [17,19]. These latter deconvolution peaks are shown in Fig. 4 by dashed lines, and their center indicates the photoluminescence energy E_{pl} of the photoemitting NPs. This value is also related to the average dimension of such NPs.

Analyzing the evolution of such signals with increasing silicon content, we can ascertain three pieces of information: (i) the intensity (area) of the peaks associated to quantum confinement, and thus the number of emitters - i.e. the NPs -, is very similar for the Si-rich samples SR4 and SR5 (the area of the PL peak associated to quantum confinement, dashed lines in Fig. 4) being only 4 % larger for SR4 compared to SR5; (ii) E_{pl} decreases, indicating larger average dimensions of the NPs, with increasing atomic Si content, but the NP size estimated from E_{pl} is very similar; (iii) the full width at half maximum (FWHM) of the signals related to the two silicon-rich samples are very similar, indicating a

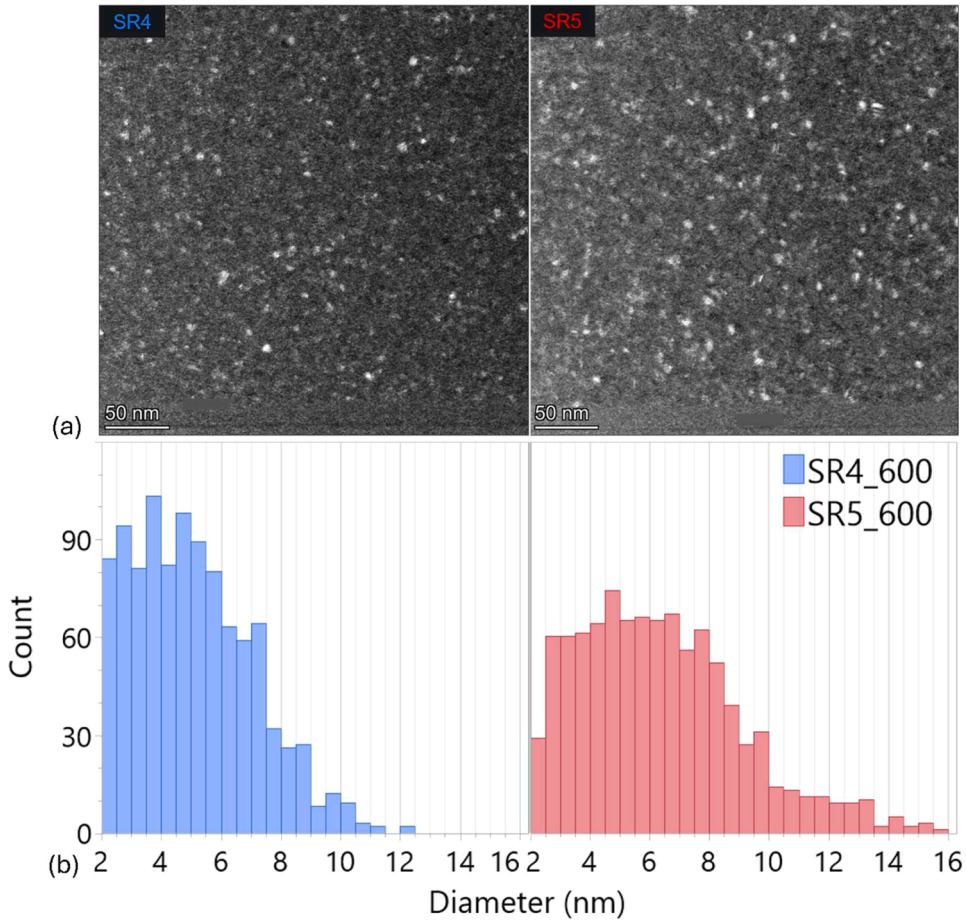

Fig. 5. after crystallization thermal treatment at 1100 °C on the two silicon rich samples, TEM analysis allowed direct observation of embedded silicon NPs inside the SiNx matrix (a). Further analysis on several TEM images permitted to estimate an average diameter and volume fraction of the NPs for the two samples (b) setting a lower selection limit of 2 nm of diameter.

similar dimensional distribution of the NPs.

Instead, we observe that the total intensity of the PL spectra is very different among the 3 samples, indicating very different radiative recombination mechanisms associated with the defect chemistry. These observations will be further elaborated in the discussion section.

Further proof of the NPs presence in the two silicon-rich films was obtained by TEM analysis. Amorphous Si NPs could not be distinguished from the bulk material in as-deposited SiN_x; thus, the three samples were subjected to a thermal annealing at 1100 °C to promote crystallization of the nanoparticles [19,31,33]. TEM analysis performed after annealing (Fig. 5a) revealed no heterogeneities in the St sample and confirmed a clear presence of NPs in the two silicon-rich samples distributed throughout the bulk matrix. To better characterize these nanoparticles, multiple images were obtained for each sample implementing post process data analysis with the software ImageJ [34]. This allowed us to distinguish each nanoparticle via grey-scale optical filtering, modeling them with spherical shapes, and performing statistical evaluation of their average dimension (Fig. 5b) and volume dispersion, by knowing the thickness of the TEM lamellas. Moreover, the TEM images were taken both from the surface of the deposited film and from the bottom (the latter reported in Fig. 5), allowing to ascertain the absence of significant gradients of the NPs distribution across the bulk thickness. It is possible to observe NPs of similar average diameter and volume fraction, with SR5 showing values of 5.36 nm and 1.13 %, respectively, slightly higher than SR4 showing values of 5.06 nm and 0.98 %, respectively.

This crystallization process was carried out mainly to have visual confirmation by TEM of the actual presence of NP heterogeneities in the silicon-rich films. Moreover, since it was performed identically on the different samples, it is plausible that the variation in the average diameter of the NPs after treatment is also similar. This allows us to assume that a similar size of crystalline NPs, both in diameter and in volume fraction, could indicate a similar relationship in the case of amorphous NPs.

To further strengthen this hypothesis, a phenomenological relation proposed by Kim et.al [35] and Park et.al [36], which correlates E_{pl} and average diameter of PL emitting amorphous silicon nanoparticles, was used:

$$d_a = \sqrt{\frac{2.40}{E_{pl} - 1.56}} \tag{2}$$

where E_{pl} (eV) is the photoluminescence energy and d_a (nm) is the average diameter of the NPs. Applying the formula, it is possible to make a size estimation of the amorphous NPs prior to the thermal treatment and to compare the obtained values with those measured from the TEM images. All results are reported in Table 1.

This analysis brings three main results: (i) the average size and volume fraction (V_{NPs}/V_{Tot}) of the crystalline NPs appear to weakly vary with increasing silicon content; (ii) the difference in average NPs size between SR4 and SR5 is higher for the amorphous NPs (+16 %) with respect to the crystalline one (+6 %); (iii) the average sizes of the NPs are larger after the crystallization thermal treatment. This last phenomenon could be induced by clustering effects promoted above ~750 °C [37], which could lead to atom migration or smaller NPs merging during crystallization to form larger ones.

These results suggest that, as sizes and distributions of the crystalline NPs are similar between the two silicon-rich samples, a similar size distribution can be expected also for the amorphous NPs, confirming the indications obtained by PL measurements. Moreover, even considering the possible difference in the size and distribution of amorphous NPs between samples SR4 and SR5, the NP sizes are too small to indicate a potential toughening effect from crack deflection, which is a mechanism described for composite materials. However, the XPS results confirmed the presence of significantly higher amounts of silicon in the SR5 sample compared to that present in the SR4 one. Thus, it would be plausible that part of the silicon remained within the film in other forms, such as heterogeneities, interstitials atoms, or particles too small to be detected.

Table 1
parameters related to NPs embedded in SR4 and SR5 samples both extrapolated for TEM image and phenomenological expressions by Kim et.al [35] and Park et al. [36] (eq. (2)). The subscripts c and a indicate the diameter of a crystalline and amorphous NPs, respectively. The errors relative to the da values have been evaluated considering the FWHM of the deconvoluted peaks related to quantum confinements.

	SR4	SR5
Si/N Ratio	1.1 ± 0.3	1.3 ± 0.4
Volume fraction from TEM (%)	1.0 ± 0.3	1.1 ± 0.3
d_c from TEM (nm)	5.1 ± 2.0	5.4 ± 2.2
d_a from Eq (2) (nm)	2.5 ± 0.6	2.9 ± 0.5

3.2. Mechanical properties

To investigate the mechanical properties of the silicon nitride films, intrinsic residual stress, hardness, plain strain elastic modulus, and fracture toughness were measured. These mechanical properties were assessed to clarify how compositional variations influence the overall mechanical performance of SiN_x films, particularly concerning their fracture behavior.

Intrinsic residual stress values obtained by wafer curvature measurements and Stoney's equation are equal to 120 MPa (tensile) for the St sample, 15.2 MPa (tensile) for the SR4 sample and −85.3 MPa (compressive) for the SR5 sample. It is possible to observe a monotone shift in the stress state from tensile to compressive with increasing silicon content, but the quantities remain low in their absolute values for each sample, considering that PECVD silicon nitride can develop residual stresses in the order of hundreds of MPa, strongly variable depending on gas flow ratio, RF power and chamber pressure during deposition [38].

Plane strain modulus and hardness have been evaluated by indenting directly on the surface of the samples with a Berkovich tip through the classical Oliver & Pharr method, applying the Intrinsic Thin Film approach to eliminate the substrate effect; results (reported below) do not vary strongly in absolute values, but decrease linearly with increasing Si % for the reduced modulus and shows similar hardness for St and SR4 samples while showing a lower value for the SR5 sample.

Finally, the deposited films were subjected to controlled dry etching to obtain the step-like pattern necessary to apply the method developed by Xia et.al [14]. Figs. 6a and b report the linear fitting of the points obtained by plotting the crack lengths *a* (through the film coating) against the crack lengths *b* (through the free substrate) for all indentations with the different applied loads and a front-view optical image of one indentation, respectively. One explanation for the increase in the data spread at higher loads, visible in Fig. 6a, could be related to the development of cracks shape different from the radial ones, most obtained only at lower loads. Despite this, the obtained points almost always show cracks *a* shorter in length than cracks *b* – as expected from the energy balance criterion underlying the method of Xia et al. – and a linear fit clearly remains the most suitable.

It is possible to directly evaluate the value "$\varphi(b\text{-}a)$" inside Eq. (1) as the intercept of the fitting curves reported. Thus, the toughness of the three coatings can be evaluated directly from Eq. (1) by also knowing the plane strain modulus and toughness of the substrate (180 GPa and 0.7 MPa$\sqrt{m}$, respectively for [111] crystalline bulk silicon [14,39]) and adding information related to plane strain modulus and intrinsic stress obtained for the coatings. All mechanical parameters, including critical stress intensity factor, hardness, plane modulus and residual stress, are reported in Table 2.

As expected for the case of brittle failure, the standard deviations calculated for the three toughness values are large [6], however, the average obtained K_{Ic} values are in the same range of values already shared in literature for similar films analyzed with different techniques,

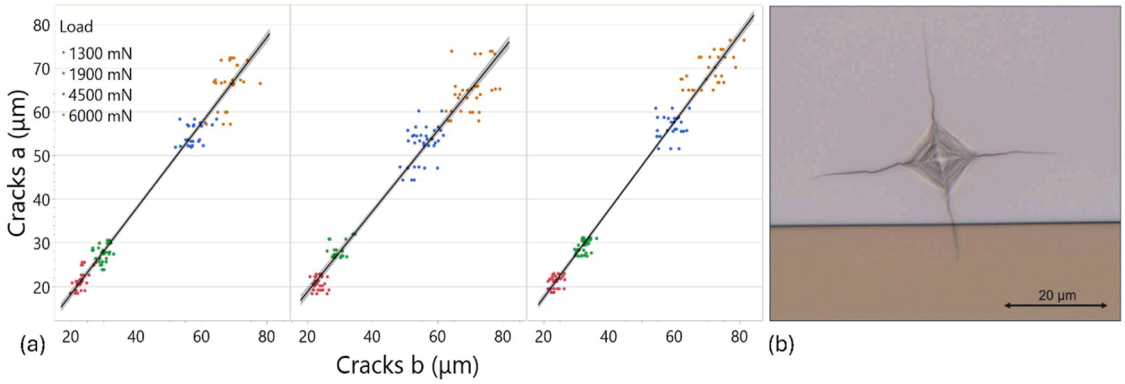

Fig. 6. coating crack lengths a vs. substrate crack lengths b at various indentation loading for St, SR4 and SR5 samples from left to right (a) and front view optical image of one indentation at 1300 mN (b).

Table 2
critical stress intensity factor (KIc), hardness (H), reduced elastic modulus (Ep) and residual stress (σ) of the three analyzed samples.

	K_{Ic} $[MPa\sqrt{m}]$	H $[GPa]$	E_p $[GPa]$	σ $[MPa]$
St	1.45 ± 0.38	15.47 ± 1.03	150 ± 2.26	120.1
SR4	1.12± 0.46	15.77 ± 0.13	138 ± 2.06	15.2
SR5	2.23 ± 0.32	13.47 ± 0.23	125 ± 3.53	−85.3

such as micro-cantilever deflection [11] or estimated numerically [40]. The St and SR4 films show average toughness values so similar to be statistically indistinguishable from one another. In contrast, SR5 sample displays a significantly larger toughness, indicating that the silicon content is related to a toughening effect over a critical threshold.

Finally, Fig. 7 shows how the fracture toughness and the hardness of the three samples analyzed display a trade-off - i.e., larger toughness corresponds to smaller hardness - as has been observed phenomenologically in other previous studies [16,41].

The SR4 film exhibits the highest hardness values, similar to that of the Standard sample, suggesting higher yield strength, which complies with a more brittle post-elastic behavior. In contrast, the SR5 sample shows lower hardness suggesting lower yield strength, hence higher chances to dissipate excessive strain energy via plastic deformation rather than only crack initiation and propagation. These aspects further corroborate a different mechanical behavior of the SR5 sample from the Standard and SR4 samples.

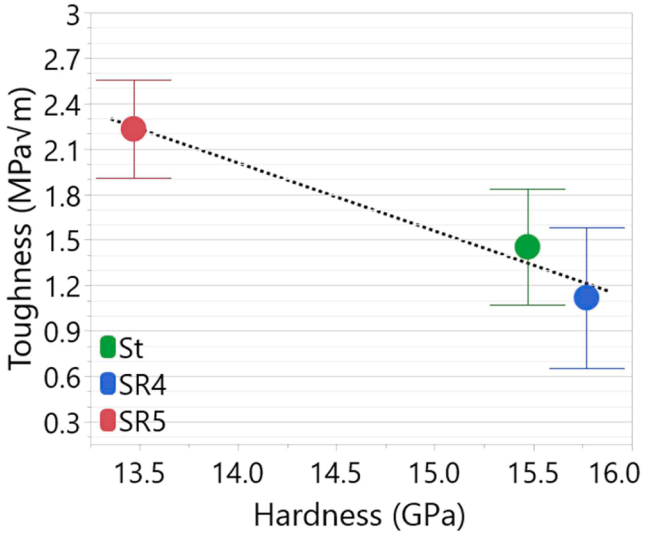

Fig. 7. fracture toughness vs. hardness for the three analyzed SiNx film. A linear relation between the two values has been observed, as already indicated in similar studies. Standard error of toughness evaluation is reported.

4. Discussion

The main objective of this research was to understand if and how the variation of SiN_x stoichiometry during PECVD synthesis impacts its mechanical properties. The results have shown that a toughening effect is indeed possible when depositing SiN_x coatings with a sufficiently high ratio between the flux of silane and ammonia, i.e., a strong enough over-stoichiometry of silicon in the film composition. However, it is not straightforward to understand the exact mechanisms behind such variation in the mechanical behavior of silicon nitride.

Our results showed the formation of amorphous NPs only for the two silicon rich samples, both proved by Raman and PL analysis, and by direct visualization by TEM imaging after the crystallization thermal treatment. The properties of these amorphous silicon clusters are very similar in the SR4 and SR5 samples, both in terms of average size, size variability, and quantity, as observed from the photoluminescence results. The distribution analysis by TEM images provides further confirmation on the similarity between the NPs in the two samples: although the crystallized particles will differ from the amorphous ones, the heat treatment, applied identically to both samples, should modify them in a similar way. This information indicates that the presence of NPs cannot explain the difference in toughness between the two silicon-rich samples, and thus neither between the SR5 and St samples.

A variation of the intrinsic stress generated during deposition from compressive to tensile with increasing silicon content has also been observed. The development of tensile intrinsic stress can certainly increase the effective toughness, even though the stress variation is quite low to explain alone the toughness variation observed for the SR5 sample. Hardness is instead very similar between the St and SR4, while it decreases significantly in the most Si-rich film SR5. This reduction in hardness suggests lower yield strength, hence higher room for energy dissipation via plasticity in the post-elastic regime, which would explain the observed increase in fracture toughness.

On top of these considerations, the XPS results clearly show that the SR5 sample has a significantly higher atomic percentage of silicon (Si/N ratio equal to 1.33) compared to the SR4 sample (which is only slightly over-stoichiometric) and the St sample (slightly sub-stoichiometric).

This means that all Si-rich films contain amorphous Si nanoparticles, however, increasing significantly the silicon content during the PECVD growth of a SiN_x film does not lead to an increase in the size or concentration of segregated Si nanoparticles, but rather to an excess of silicon which remains dispersed as interstitial atoms, Si atom bonded to N (e.g. filling dangling bonds) or as very small clusters (not contributing to PL), impacting in a stronger way the mechanical properties of the SiN_x matrix. Interstitial atoms can modify the intrinsic stress evolution during

growth and amorphous clusters are known to possess lower hardness compared to stoichiometric silicon nitride [41], thus, their incorporation into the matrix may be expected to facilitate localized plasticity, thereby enhancing fracture resistance.

Even though the exact mechanisms relating to local atomic structure and mechanical properties certainly require further investigation, this can explain why an excessive amount of dispersed silicon would lead to a reduced hardness of the SiN_x matrix and a shift toward compressive stress formation simultaneously, thus leading to an increase in the effective toughness of the material.

5. Conclusions

This work provided a comprehensive characterization and evaluation of the mechanical properties of silicon nitride thin films deposited via PECVD, focusing on how chemical composition influences fracture toughness. Three films with varying silicon content - standard (quasi-stoichiometric), silicon-rich SR4, and silicon-rich SR5 - were analyzed through structural and mechanical characterization techniques.

Intrinsic residual stress measurements revealed a shift from tensile to compressive states with increased silicon content, though the absolute values remained moderate and insufficient alone to fully explain the observed mechanical performance differences. Structural and optical characterizations via XPS, Raman, and PL spectroscopy confirmed the presence of embedded amorphous silicon nanoparticles in silicon-rich films, which are however similar in average dimension with varying stoichiometry, as also inferred by TEM analyses following thermal annealing.

Fracture toughness evaluation through the method proposed by Xia et al. demonstrated that the SR5 composition exhibited higher toughness compared to the SR4 and St SiN_x films. Interestingly, hardness analysis indicated a lower value for SR5, suggesting decreased yield strength. The inverse relationship between hardness and toughness observed aligns with previous phenomenological findings reported in the literature.

Given the small nanoparticle sizes observed and their similarities between the two silicon-rich samples, traditional toughening mechanisms typically attributed to nanoparticle heterogeneities in composite materials cannot fully account for the enhanced toughness in the SR5 SiN_x film. Instead, it is proposed that the excess amount of silicon in the SR5 sample compared to SR4 is dispersed in the SiN_x matrix as heterogeneities different from the observed clusters, such as interstitial atoms or replacing the dangling bonds typically present in SiN_x, reducing the effective hardness and altering intrinsic stress development during deposition, contributing to the enhanced fracture toughness.

Overall, these results indicate that carefully tuning the silicon content and thus modifying the internal microstructure of PECVD SiN_x films represents a possible strategy to control and enhance mechanical properties which are critical for device reliability. Future research should further explore the detailed mechanisms underpinning the effect of amorphous silicon dispersions on different properties, for example regarding their impact on conductivity, to enable tailored optimization of SiN_x passivation layers for specific semiconductor applications.

CRediT authorship contribution statement

Filippo Sabatini: Writing – review & editing, Writing – original draft, Methodology, Investigation, Formal analysis, Data curation, Conceptualization. **Emanuele Cattarinuzzi:** Writing – review & editing, Methodology, Conceptualization. **Vincent Coutellier:** Writing – review & editing, Supervision, Conceptualization. **Andrea Serafini:** Writing – review & editing, Methodology, Investigation. **Simone Mariani:** Writing – review & editing, Validation, Supervision. **Davide Fagiani:** Writing – review & editing, Validation, Supervision. **Laurent-Luc Chapelon:** Writing – review & editing, Resources. **Paola Zuliani:** Writing – review & editing, Supervision, Funding acquisition. **Andrea Li Bassi:** Writing – review & editing, Supervision, Funding acquisition, Conceptualization.

Declaration of competing interest

The authors declare that they have no known competing financial interests or personal relationships that could have appeared to influence the work reported in this paper.

Acknowledgements

The authors would like to express their gratitude to ST Microelectronics and Politecnico di Milano for their invaluable support and collaboration in this research. This work was carried out as part of a joint effort between the two institutions, combining academic and industrial expertise to achieve the presented results. The authors also acknowledge the contributions of all team members involved in this project. Furthermore, the authors thank Enrica Ravizza (STMicroelectronics Agrate) for her important contribution in carrying out the XPS analyses and all members of *FMT Physical Laboratory* of STMicroelectronics Agrate who have sustained this research with their invaluable support.

Filippo Sabatini acknowledges the Italian Ministry of University and Research (MUR) under the National Recovery and Resilience Plan (PNRR), Mission 4, Component 2, Investment 3.3, through the Ministerial Decree n.352 for partially funding this research.

References

[1] N. Hegedüs, K. Balázsi, C. Balázsi, Silicon nitride and hydrogenated silicon nitride thin films: a review of fabrication methods and applications, Materials. (Basel) 14 (19) (2021) 5658.
[2] O.P. Agnihotri, S.C. Jain, J. Poortmans, J. Szlufcik, G. Beaucarne, J. Nijs, R. Mertens, Advances in low temperature processing of silicon nitride baseddielectrics and their applications in surface passivation and integratedoptical devices, Semicond. Sci. Technol. 15 (7) (2000). R29.
[3] J. Seiffe, L. Gautero, M. Hofmann, J. Rentsch, R. Preu, S. Weber, R.A. Eichel, Surface passivation of crystalline silicon by plasma-enhanced chemical vapor deposition double layers of silicon-rich silicon oxynitride and silicon nitride, J. Appl. Phys. 109 (3) (2011).
[4] B. Arkles, C. Brick, J. Goff, A.E. Kaloyeros, Simplified CVD route to near-zero thickness silicon nitride films, J. Vacuum Sci. Technol. B 40 (4) (2022).
[5] Y.C. Huang, S.Y. Chang, C.H. Chang, Effect of residual stresses on mechanical properties and interface adhesion strength of SiN thin films, Thin. Solid. Films. 517 (17) (2009) 4857–4861.
[6] T.L. Anderson, T.L. Anderson, Fracture mechanics: Fundamentals and Applications, CRC press, 2005, pp. 257–293.
[7] J. Ast, M. Ghidelli, K. Durst, M. Göken, M. Sebastiani, A.M. Korsunsky, A review of experimental approaches to fracture toughness evaluation at the micro-scale, Mater. Des. 173 (2019) 107762.
[8] S. Zhang, X. Zhang, Toughness evaluation of hard coatings and thin films, Thin. Solid. Films. 520 (7) (2012) 2375–2389.
[9] R. Saha, W.D. Nix, Effects of the substrate on the determination of thin film mechanical properties by nanoindentation, Acta Mater. 50 (1) (2002) 23–38.
[10] T.Y. Tsui, G.M. Pharr, Substrate effects on nanoindentation mechanical property measurement of soft films on hard substrates, J. Mater. Res. 14 (1) (1999) 292–301.
[11] K. Matoy, H. Schönherr, T. Detzel, T. Schöberl, R. Pippan, C. Motz, G. Dehm, A comparative micro-cantilever study of the mechanical behavior of silicon based passivation films, Thin. Solid. Films. 518 (1) (2009) 247–256.
[12] L. Chen, K. Zeng, Y. Zhang, C. She, G. Liu, A new approach to determine wedge-indented interfacial toughness in soft-film hard-substrate systems with application to low-k films on Si substrate, J. Mater. Res. 27 (22) (2012) 2872–2883.
[13] K.R. Morasch, D.F. Bahr, An energy method to analyze through thickness thin film fracture during indentation, Thin. Solid. Films. 515 (6) (2007) 3298–3304.
[14] Z. Xia, W.A. Curtin, B.W. Sheldon, A new method to evaluate the fracture toughness of thin films, Acta Mater. 52 (12) (2004) 3507–3517.
[15] S. King, R. Chu, G. Xu, J. Huening, Intrinsic stress effect on fracture toughness of plasma enhanced chemical vapor deposited SiNx: h films, Thin. Solid. Films. 518 (17) (2010) 4898–4907.
[16] Z. Gan, C. Wang, Z. Chen, Material structure and mechanical properties of silicon nitride and silicon oxynitride thin films deposited by plasma enhanced chemical vapor deposition, Surfaces 1 (1) (2018) 59–72.
[17] T.V. Torchynska, J.C. Espinola, E.V. Hernandez, L. Khomenkova, F. Delachat, A. Slaoui, Effect of the stoichiometry of Si-rich silicon nitride thin films on their photoluminescence and structural properties, Thin. Solid. Films. 581 (2015) 65–69.

[18] L.V. Mercaldo, E.M. Esposito, P.D. Veneri, G. Fameli, S. Mirabella, G. Nicotra, First and second-order raman scattering in Si nanostructures within silicon nitride, Appl. Phys. Lett. (15) (2010) 97.
[19] W. Liao, X. Zeng, X. Wen, X. Chen, W. Wang, Annealing and excitation dependent photoluminescence of silicon rich silicon nitride films with silicon quantum dots, Vacuum. 121 (2015) 147–151.
[20] S. Meziani, A. Moussi, L. Mahiou, F. Antoni, R. Outemzabet, Rapid thermal process for crystallization silicon nitride films, Surface Eng. 36 (5) (2020) 456–464.
[21] G.C. Janssen, M.M. Abdalla, F. Van Keulen, B.R. Pujada, B. Van Venrooy, Celebrating the 100th anniversary of the Stoney equation for film stress: developments from polycrystalline steel strips to single crystal silicon wafers, Thin. Solid. Films. 517 (6) (2009) 1858–1867.
[22] W.C. Oliver, G.M. Pharr, An improved technique for determining hardness and elastic modulus using load and displacement sensing indentation experiments, J. Mater. Res. 7 (6) (1992) 1564–1583.
[23] H. Li, J.J. Vlassak, Determining the elastic modulus and hardness of an ultra-thin film on a substrate using nanoindentation, J Mater Res 24 (3) (2009) 1114–1126.
[24] N. Jehanathan, B. Walmsley, Y. Liu, J. Dell, Oxidation of PECVD SiNx thin films, J. Alloys. Compd. 437 (1–2) (2007) 332–338.
[25] R. Liu, M. Canonico, Applications of UV-raman spectroscopy to microelectronic materials and devices, in: AIP Conference Proceedings, 683, American Institute of Physics, 2003, pp. 738–743, https://doi.org/10.1063/1.1622552.
[26] L.V. Mercaldo, P.D. Veneri, E.M. Esposito, M. Tucci, Annealing effects on aSiNx grown by PECVD using different gas mixtures, Physica Status Solidi c 7 (3–4) (2010) 832–835.
[27] J. He, C. Wang, W. Li, K.C. Qi, Y.D. Jiang, Effect of gas temperature on the structural and optoelectronic properties of a-Si: h thin films deposited by PECVD, Surface Coat. Technol. 214 (2013) 131–137.
[28] L. Giacomazzi, P. Umari, First-principles investigation of electronic, structural, and vibrational properties of a-Si 3 N 4, Phys. Rev. B—Condens. Matter Mater. Phys. 80 (14) (2009) 144201.
[29] I. Parkhomenko, L. Vlasukova, F. Komarov, O. Milchanin, M. Makhavikou, A. Mudryi, D. Murzalinov, Origin of visible photoluminescence from Si-rich and N-rich silicon nitride films, Thin. Solid. Films. 626 (2017) 70–75.
[30] L. Museur, A. Zerr, A. Kanaev, Photoluminescence and electronic transitions in cubic silicon nitride, Sci. Rep. 6 (1) (2016) 18523.
[31] M. Molinari, H. Rinnert, M. Vergnat, Evolution with the annealing treatments of the photoluminescence mechanisms in a-SiNx: h alloys prepared by reactive evaporation, J. Appl. Phys. (12) (2007) 101.
[32] A.V. Amosov, Y.N. Kulchin, A.V. Dvurechenskii, V.P. Dzyuba, Photoluminescence and excitation energy transfer in non-stoichiometric silicon nitride, J. Lumin. 243 (2022) 118615.
[33] Q. Liu, X. Chen, H. Li, Y. Guo, J. Song, W. Zhang, Z. Lin, Effect of thermal annealing on the photoluminescence of dense Si nanodots embedded in amorphous silicon nitride films, Micromachines. (Basel) 12 (4) (2021) 354.
[34] C. Igathinathane, L.O. Pordesimo, E.P. Columbus, W.D. Batchelor, S.R. Methuku, Shape identification and particles size distribution from basic shape parameters using ImageJ, Comput. Electron. Agric. 63 (2) (2008) 168–182.
[35] N.M. Park, C.J. Choi, T.Y. Seong, S.J. Park, Quantum confinement in amorphous silicon quantum dots embedded in silicon nitride, Phys. Rev. Lett. 86 (7) (2001) 1355.
[36] T.Y. Kim, N.M. Park, K.H. Kim, G.Y. Sung, Y.W. Ok, T.Y. Seong, C.J. Choi, Quantum confinement effect of silicon nanocrystals in situ grown in silicon nitride films, Appl. Phys. Lett. 85 (22) (2004) 5355–5357.
[37] J. Holm, J.T. Roberts, Sintering, coalescence, and compositional changes of hydrogen-terminated silicon nanoparticles as a function of temperature, The J. Phys. Chem. C 113 (36) (2009) 15955–15963.
[38] S.J. Oh, B.S. Ma, C. Yang, T.S. Kim, Intrinsic mechanical properties of free-standing SiN x thin films depending on PECVD conditions for controlling residual stress, ACS. Appl. Electron. Mater. 4 (8) (2022) 3980–3987.
[39] M.A. Hopcroft, W.D. Nix, T.W. Kenny, What is the Young's Modulus of Silicon? J. Microelectromechan. Syst. 19 (2) (2010) 229–238.
[40] K. Kim, H. Luo, A.K. Singh, T. Zhu, S. Graham, O.N. Pierron, Environmentally assisted cracking in silicon nitride barrier films on poly (ethylene terephthalate) substrates, ACS. Appl. Mater. Interfaces. 8 (40) (2016) 27169–27178.
[41] C. Wang, K. Shi, C. Gross, J.M. Pureza, M. de Mesquita Lacerda, Y.W. Chung, Toughness enhancement of nanostructured hard coatings: design strategies and toughness measurement techniques, Surface Coat. Technol. 257 (2014) 206–212.